

Marcus Schwäbisch, João Moreira

Aerosensing Radarsysteme GmbH  
 c/o DLR, D-82234 Oberpfaffenhofen, Germany  
 Phone: +49-8153-281350  
 Fax: +49-8153-281543  
 Email: Marcus.Schwaebisch@dlr.de

ABSTRACT

This paper presents design and applications of the high resolution airborne interferometric SAR AeS-1, built and operated by Aerosensing Radarsysteme. It operates in the X-band range and is configured as dual-antennae cross-track interferometric SAR with the main parameters: 9.6 GHz operating frequency, 400 MHz bandwidth, 1.8 m baseline, up to 14 km swath width, 0.5 m horizontal resolution, and height accuracy up to 5 cm. The system can additionally be operated in along-track interferometric mode for measuring surface currents. Currently, AeS-1 is used for a variety of applications, including the generation of high resolution digital elevation models, derivation of large scale topographic and thematic maps (up to scale 1:2000), and extraction of building heights for generation of city models. In addition to these operational modes, research studies are carried on mainly for oceanographic purposes, using ATI and cross track mode for imaging of the ocean surface, bathymetry estimation and real-time SAR observation of coastal areas.

1 INTRODUCTION

The high resolution airborne synthetic aperture radar AeS-1, designed and manufactured by Aero-Sensing Radarsysteme GmbH, is configured as a two-antennae single-pass interferometric SAR with a ground resolution up to  $0.5 \text{ m} \times 0.5 \text{ m}$  and a height accuracy up to 5 cm. The system was first flown in August 1996 and is in operational use since October 1996. In typical flight campaigns, data covering several thousands of  $\text{km}^2$  are acquired, processed to georectified digital elevation models and radiometrically calibrated SAR

\*Presented at the Fourth International Airborne Remote Sensing Conference and Exhibition/21st Canadian Symposium on Remote Sensing, Ottawa, Ontario, Canada, 21-24 June 1999.

magnitude images, and finally post-processed to value-added products like height contour maps, topographic map sheets, or city models.

This paper gives a technical description of the concept, end-to-end design as well as the data processing chain of AeS-1. In the following section the ground and flight segments of the system are described, section 3 presents the data processing flow along with the product generation, and finally an outlook on future concepts concludes the paper.

2 AES-1 SYSTEM

The AeS-1 system consists of a ground and a flight segment. The block diagram in Fig. 1 shows their components and interconnections.

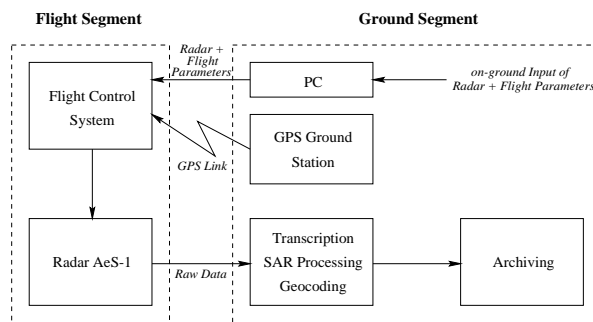


Figure 1: Block diagram of AeS-1 ground and flight segments

2.1 GROUND SEGMENT

The ground segment is divided into the following sub-systems:

- *Laptop computer for flight planning:* the operator enters the flight track coordinates and selects the radar parameters (like resolution and swath width).
- *Transcription system:* transcription of the recorded raw data on a disk array system to Digital Linear Tapes (DLT) with 35 GBytes storage capacity. Additionally, the D-GPS/Inertial Navigation System (INS) data of the flight are processed and synchronized with the radar raw data.
- *SAR and InSAR processing:* reading of the raw data from the DLTs, data processing, and re-writing the resulting products onto DLT tapes. The processing is realized by an array of PCs interconnected by a fast Ethernet network. One PC can process a  $2 \text{ km} \times 2 \text{ km}$  full resolution dataset in 16 hours generating the following products automatically:
  - terrain-geocoded elevation model with a height accuracy up to 5 cm (depending on the ground resolution of the terrain model)
  - terrain-geocoded and radiometrically calibrated SAR image with a ground resolution of  $0.5 \text{ m} \times 0.5 \text{ m}$
  - terrain-geocoded coherence map

Products with lower height and ground resolution need less processing time.

- *Archiving:* management of the raw data and image products archiving using a sophisticated man-machine interface for job generation and job control.
- *GPS ground station:* it consists of a high performance two-frequency GPS receiver and a radio data link to the aircraft allowing real time kinematic D-GPS tracing during the flight. The data received by the ground station are additionally recorded for later high precision off-line D-GPS processing. For achieving a DEM height accuracy of 5 cm the fixed differential GPS solution by off-line D-GPS processing and a maximum range between aircraft and ground station are required.

## 2.2 FLIGHT SEGMENT

The flight segment of the AeS-1 system consists of the following subsystems (Figs. 2, 3):

- *Antennas:* each one has a weight of 3 kg and a size of W: 36 cm, H: 13 cm, D: 15 cm. They are



Figure 2: Turbine Commander with antenna boom construction



Figure 3: AeS-1 flight segment

mounted on the fuselage by means of a rigid boom construction (Fig. 2) in order to minimize possible variations of their position relative to each other as well as to the INS. The effective interferometric baseline length is optionally 0.5 m or 1.8 m.

- *Transmitter/receiver:* the transmitter/receiver uses a high precision local oscillator, a digital chirp generator and a TWT based output amplifier. High speed circulators allow a fully interferometric operation up to a pulse repetition frequency of 16 kHz.
- *Clock generator, control computer and disk array unit:* the control computer controls the transmitter, receiver, clock generator, and disk array units and is, in turn, controlled by the flight control system. The maximum recording data rate for each unit is 32 MByte/s. Each of the 3 disk arrays has a storage

capacity of 144 GByte.

- *Flight control system:* the flight control system is based on an on-line kinematic D-GPS system coupled with an inertial navigation system (INS). The GPS data of the ground station is received and processed in real-time.

The main system parameters of the AeS-1 flight segment are summarized in Tab. 1.

Table 1: System Parameters of AeS-1 Flight Segment

System Parameters of AeS-1 Flight Segment	
Operating Frequency	9.35...9.75 GHz
System Bandwidth	400 MHz
PRF	up to 16 kHz
Ground Resolution	up to 0.5 m × 0.5 m
Swath Width	1...15 km
Flight Velocity	50...200 m/s
Typical Flight Altitude	500...9000 m
InSAR Baseline	0.5 or 1.8 m
Dimensions	W: 1.1 m, H: 1 m, D: 0.6 m
Weight	200 kg including antennas
Power	28 V, 60 A maximum

Due to its compact design it can be installed on rather small aircrafts. Up to now a Cessna 207A, a Dornier 228, an Aerocommander 685, and a Turbine Commander (Fig. 2) have been served as carrier platform.

AeS-1 is a fully automatic system. The flight control unit includes a display where the real track and its deviation relative to the nominal one are indicated. The pilot simply has to follow the displayed track, no co-pilot or operator is necessary. The aircraft position is delivered in real-time with an absolute accuracy of 1 m, which allows the pilot to keep the position error between real and nominal track below 10 m during the entire flight.

The installation of the AeS-1 flight segment in an unprepared aircraft can be carried out within a period of 1 week. In a prepared aircraft the installation takes a couple of hours.

### 3 DATA PROCESSING AND PRODUCT GENERATION

Fig. 4 gives an overview over the entire data processing chain from raw data selection up to final image product delivery. It can thematically be divided into 3 parts:

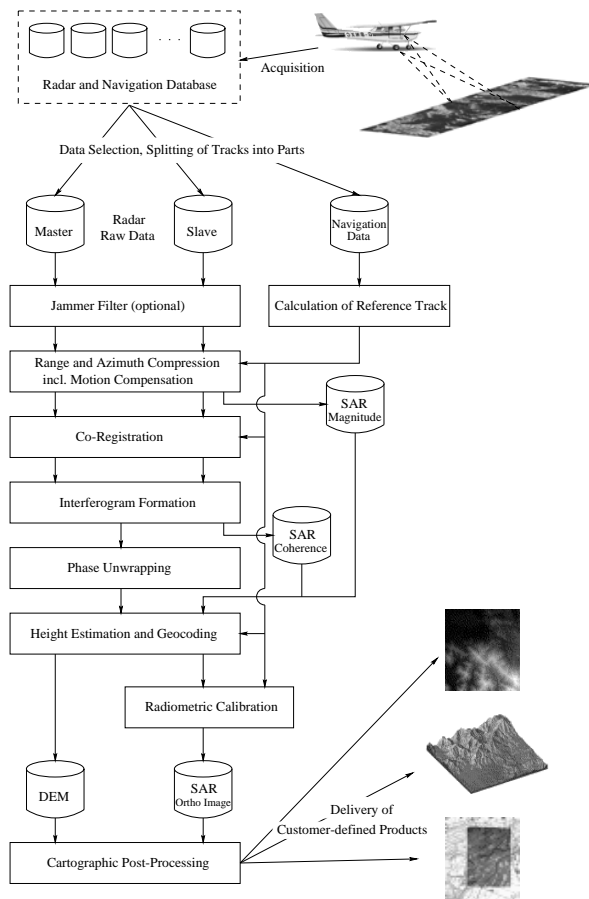


Figure 4: Data processing chain

SAR processing, interferometric processing, and cartographic processing.

#### 3.1 SAR PROCESSING

SAR processing starts with reading of the radar and navigation data from the DLTs and subsequent determination of the reference flight tracks. Using a range/Doppler processing algorithm, both datasets are compressed (including precise motion compensation) into single-look complex SAR images. For generating long image strips (> 5 km) the continuous raw data stream is splitted into overlapping parts. Optionally, the raw data can pass through a jammer filter if corresponding disturbances are present.

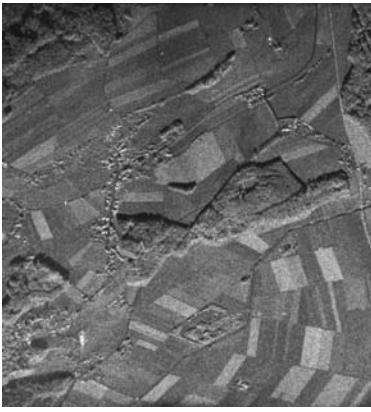


Figure 5: Amplitude

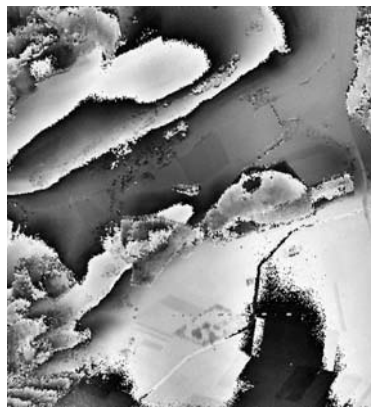


Figure 6: Interferometric phase

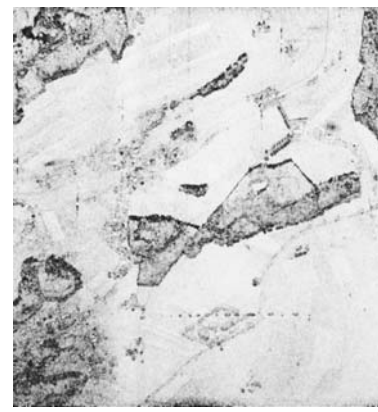


Figure 7: Coherence

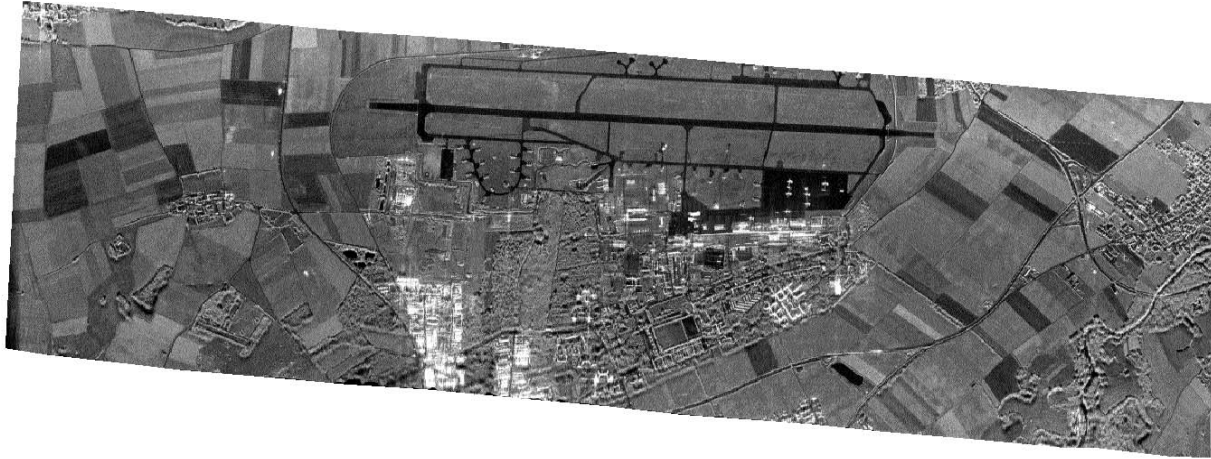


Figure 8: SAR orthoimage of Fürstenfeldbruck airfield (8.7 km × 2.8 km)

### 3.2 INTERFEROMETRIC PROCESSING

The interferometric processor carries out the co-registration of the images, the interferogram formation, the phase unwrapping, and finally the phase-to-height conversion. Image products are SAR magnitude, interferogram, coherence map, and elevation in slant range geometry. Whole image strips are produced by concatenating the individually processed parts. Details of some of the processing steps are reported in [1][2][3][4].

Figs. 5, 6, and 7 show examples of SAR magnitude, phase, and coherence, respectively, from a test site in Switzerland, covering an area of about 2 × 2 km near the village of Küttighofen.

### 3.3 CARTOGRAPHIC PROCESSING

Cartographic processing includes the projection of the slant range image products onto a cartographic reference frame as well as, in an optional further post-processing step, the generation of value-added products. According to the specific user requirements image products are delivered in different sizes/resolutions by operating the system in the corresponding swath/resolution mode. Tab. 2 gives an overview over the different options.

In the following paragraphs examples for typical end-products are given.

- *geocoded and radiometrically calibrated SAR magnitude*: In Fig. 8 a 8.7 km × 2.8 km terrain-geocoded image strip covering the Fürstenfeld-

Table 2: AeS-1 operating modes

Physical Parameter	Operating Mode				
	A	B	C	D	E
Spatial Resolution (m)	0.5...2.0	0.5...2.0	0.5...2.0	1.0...2.0	2.0...5.0
Height Accuracy (m)	0.05...0.5	0.05...0.5	0.2...0.7	0.5...1.0	1.0...2.0
Swath Width (km)	1	2	4	7.4	14.8
Radiometric Resolution (dB)	<1.8	<1.8	<1.8	<1.8	<1.8
Imaging Throughput ( $km^2/h$ )	400	800	1600	3200	6500

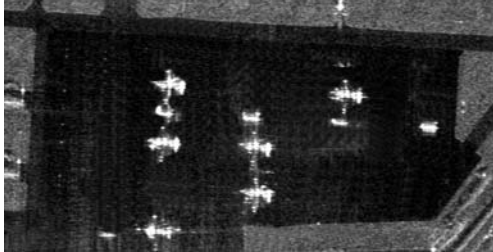


Figure 9: Aircrafts at Fürstenfeldbruck airfield (480 m  $\times$  250 m)



Figure 10: Hangars at Fürstenfeldbruck airfield (400 m  $\times$  350 m)

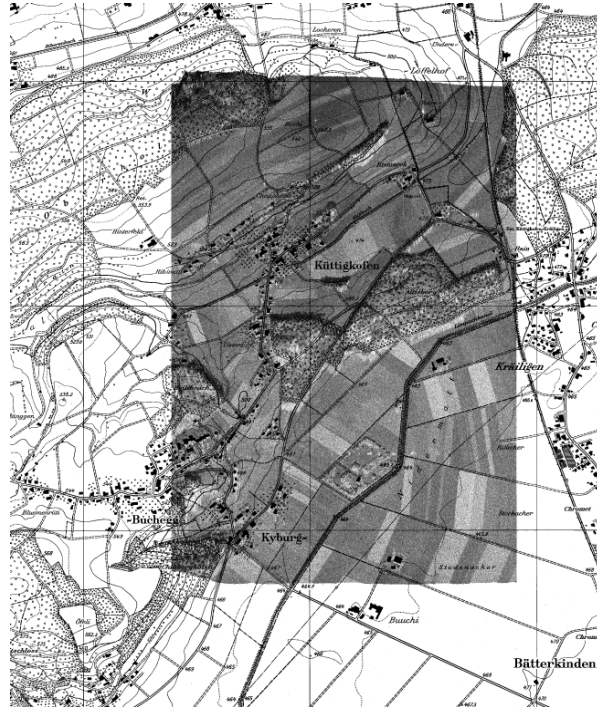


Figure 11: Terrain-geocoded SAR scene of Küttighofen with superimposed topographic map (©Vermessungsamt des Kantons Bern, Switzerland)

bruck airfield, Germany, is displayed. Two close-ups in Figs. 9 and 10 illustrate the system's high spatial resolution of 0.5 m. Fig. 11 shows the georectified magnitude of the Küttighofen scene (see Fig. 5). In order to demonstrate the geometrical accuracy a part of the swiss topographic map 1:25000 has been superimposed. Radiometric calibration is carried out according to the customer's requirements either by compensating for elevation antenna pattern and  $R^3$  dependence or by additionally removing terrain slope-induced effects.

- *geocoded DEM*: Fig. 12 gives an example of a DEM acquired in Irian Jaya, Indonesia. Hilly terrain like this has to be mapped from different directions to close possible gaps caused by layover or shadow present in single observations.

In Fig. 13 a high precision elevation model of the waddensea area in northern Germany is shown. A comparison with terrestrially measured height profiles proved an overall accuracy of 20 cm.

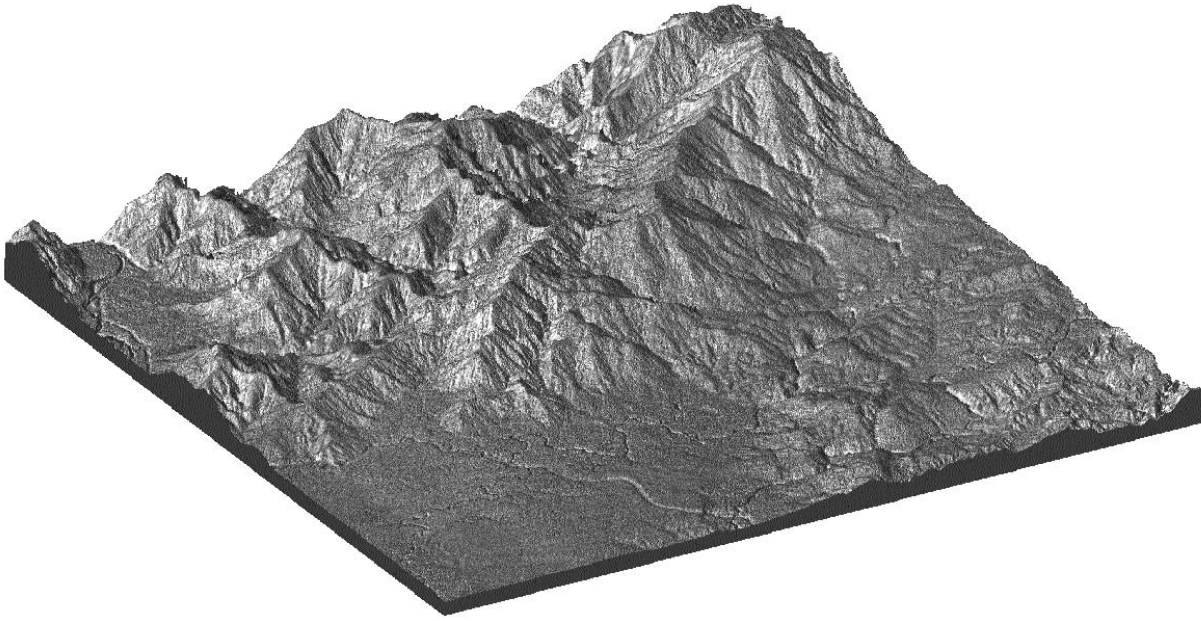


Figure 12: Perspective view of DEM, Irian Jaya, Indonesia (14 km × 14 km)

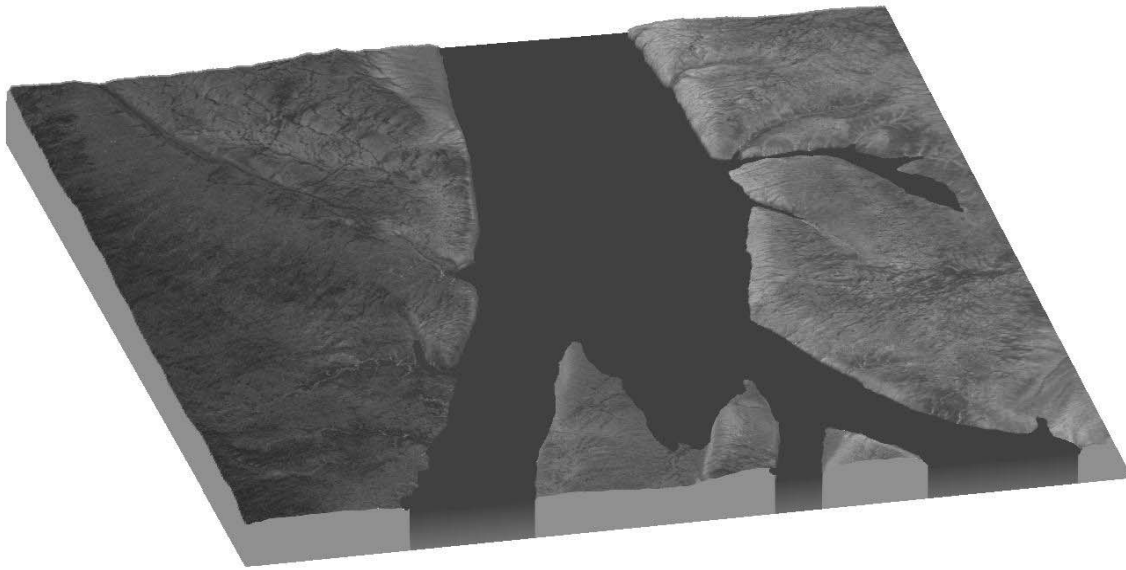


Figure 13: Elevation model of waddensea area in northern Germany

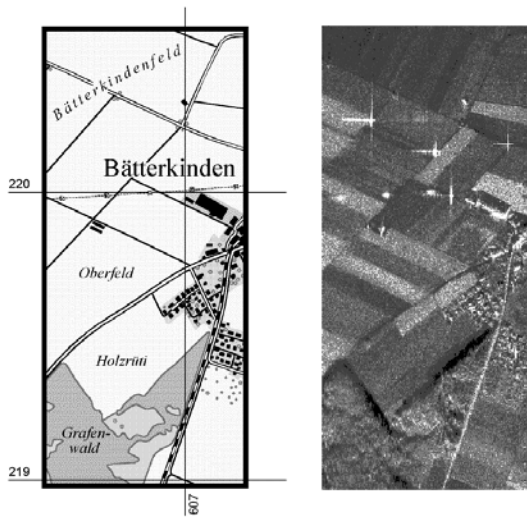


Figure 14: Topographic map and corresponding SAR amplitude of the village of Bätterkinden, Switzerland

- *topographic maps*: the production of topographic maps requires both the geocoded SAR image and DEM and comprises the following processing steps:
    1. SAR orthoimages and digital elevation models are first analyzed by co-occurrence, wavelet, and neuronal network algorithms. The classification yields the 4 independent classes water, forest, urban areas, and agricultural areas.
    2. Classification results are vectorized separately in DXF format and passed to a cartographic software.
    3. Final composition of the topographic map is accomplished manually by a cartographer. The topographic map is delivered in digital form, typically consisting of 10...30 layers in vector format.
- Fig. 14 shows amplitude along with topographic map (scale 1:25000) derived from the interferometric SAR data of the Küttighofen scene. Topographic maps in a scale up to 1:2000 can be generated by using SAR datasets with  $0.5 \text{ m} \times 0.5 \text{ m}$  ground resolution.
- *city models*: city models are generated by exploiting interferometric phase and SAR amplitude in slant range instead of map projection since the effects of multiple scattering in urban areas usually impede an automatic phase unwrapping. If avail-

able, additional sources of information like aerial photographs or cadastral maps are incorporated. The final product is composed manually by a cartographer. Fig. 15 gives an example which shows a  $1.8 \text{ km} \times 2.3 \text{ km}$  section of the central part of the city of Berlin, Germany. Horizontal resolution is 5 m, building height accuracy is approximately 3 m.

#### 4 OUTLOOK

A severe limitation of interferometric height estimation with X-Band radar is given by the fact that elevation of the terrain surface (including vegetation height) instead of the pure ground is measured. In order to overcome this principal restraint a second radar module operating in the P-Band range at 415 MHz center frequency has been added to the AeS-1 core system. First results obtained by test flights in Switzerland have demonstrated its principal capability to penetrate the vegetation canopy and measure the ground topography by operating the system in repeat-pass interferometric mode [5]. Together with the X-Band part, AeS-1 now provides the opportunity to derive elevation models for a wide range of applications by combining the high resolution of the X-Band products with the penetration characteristic of the P-Band part.

#### 5 REFERENCES

- [1] J. Moreira, "Design of an Airborne Interferometric SAR for High Precision DEM Generation," in *Proceedings of XVIII ISPRS Congress*, vol. XXI, Part B2, Commission II, (Wien), pp. 256–260, 1996.
- [2] F. Holecz, J. Moreira, P. Pasquali, S. Voigt, E. Meier, and D. Nüesch, "Height Model Generation, Automatic Geocoding and Mosaicing Using Airborne AeS-1 InSAR Data," in *Proceedings of IGARSS'97*, (Singapore), pp. 1929–1931, 1997.
- [3] A. Reigber and J. Moreira, "Phase Unwrapping by Fusion of Local and Global Methods," in *Proceedings of IGARSS'97*, (Singapore), pp. 869–871, 1997.
- [4] F. Holecz, P. Pasquali, J. Moreira, and D. Nüesch, "Rigorous Radiometric Calibration of Airborne AeS-1 InSAR Data," in *Proceedings of IGARSS'98*, (Seattle), pp. 2442–2444, 1998.
- [5] C. Hofmann, M. Schwäbisch, S. Och, C. Wimmer, and J. Moreira, "Multipath P-Band Interferometry - First Results," in *Proceedings of the Fourth International Airborne Remote Sensing Conference*, (Ottawa), 1999.

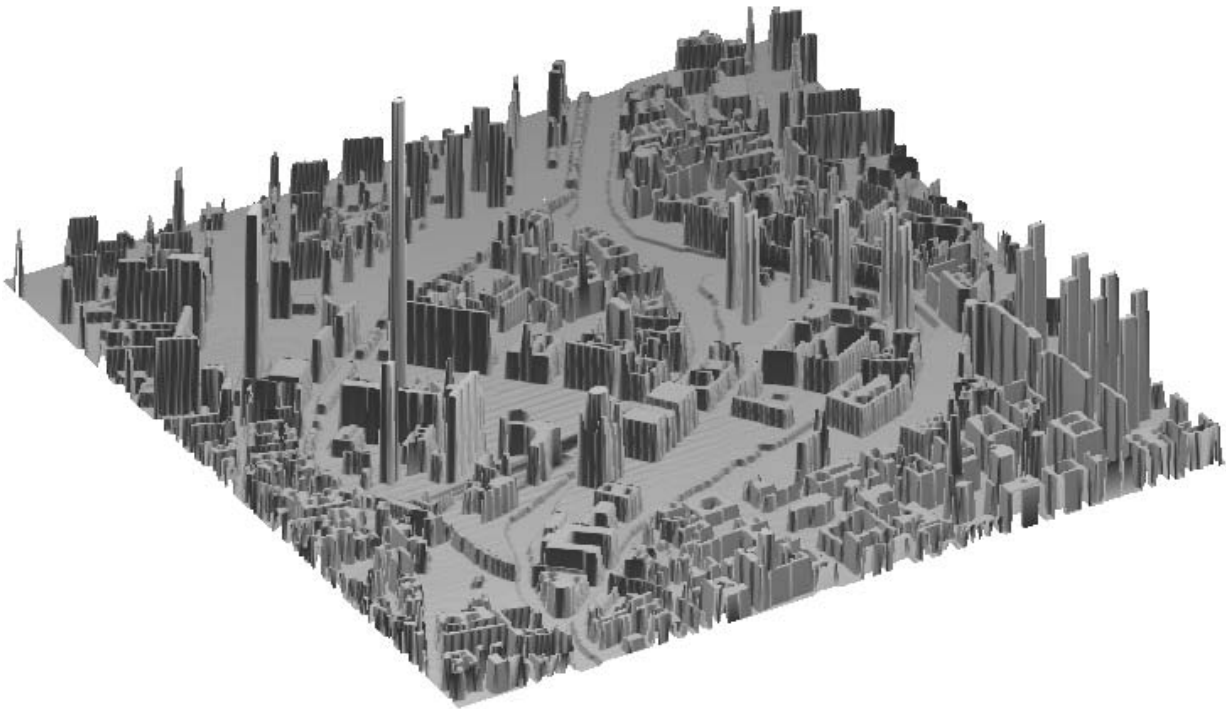


Figure 15: City model of the central part of Berlin, Germany